Spatial ordering of primary defects at elevated temperatures

A. A. Semenov and C. H. Woo
Department of Electronic and Information Engineering, The Hong Kong Polytechnic University, Hung Hom, Kowloon, Hong Kong
(Received 3 June 2004; revised manuscript received 12 November 2004; published 22 February 2005)

We consider the microstructure evolution of a nonequilibrium system of primary defects, in which mobile point defects, vacancy loops, and sessile interstitial clusters are continuously produced by cascade-damage irradiation. It is shown that in a fully annealed metal, a spatially homogeneous microstructure may become unstable if the yield of vacancy clusters in collision cascades is sufficiently low. Unlike cases studied in the literature, in which sessile interstitial clusters are not produced, we found that the instability condition can only be satisfied for a finite period of time, the duration of which depends on the density of the network dislocation. Spatial heterogeneity starts to form from a homogeneous vacancy loop population, leading to the eventual accumulation of almost all vacancy clusters within very sharp walls. The spatial distribution of interstitial clusters, on the other hand, is relatively homogeneous, simply following the spatial variations of the net interstitial flux. The spatial heterogeneity develops with the growth of some concentration peaks and the disappearance of others. As a result, the surviving peaks form an increasingly well-defined periodic structure. Nevertheless, as the total sink density of interstitial clusters and loops becomes sufficiently large, the periodic structure disappears, and spatial homogeneity of damage microstructure eventually returns.

DOI: 10.1103/PhysRevB.71.054109 PACS number(s): 61.80.Az, 61.72.Cc, 61.72.Ji

I. INTRODUCTION

The damage microstructure caused by the continuous production of lattice defects in solids under irradiation is a typical example of a system far from the equilibrium. Bifurcations in the evolution of such systems often lead to the qualitative changes in the system behavior, resulting in pattern formation[1–5] via spatial and temporal self-organization in the defect populations. Examples are bubble and void lattices,[6,7] defect walls,[8–15] and various arrays of dislocation loops and stacking fault tetrahedra.[16–18]

Pattern formation due to the development of instability in the homogeneous vacancy loop population is one of the most actively studied cases. Investigations within the reaction-diffusion mode[16,19–26] progress from the simplest case, in which only vacancy clusters, beside the Frenkel pairs, are considered,[20,21] to the more complicated cases that also include extended defects like interstitial loops and voids.[22–25] Krishan[6] showed numerically that under the continuous generation of vacancy clusters, the spatially homogeneous evolution of the damage microstructure may become unstable. Numerical calculations in the one-dimensional case further demonstrated that the development of this instability leads to the spatial ordering of vacancy loops.[20] Analytical studies[21–24] in the weakly nonlinear regime, as well as numerical simulations in two dimensions,[24] show that the evolution of a homogeneous vacancy loop population is sometimes unstable, leading to the formation of planar wall defect structures, after transients corresponding to three-dimensional patterns. Taking into account interstitial loops and voids in the reaction-diffusion model does not change this conclusion. Only the instability conditions are modified.[21–25] Thus, the necessary conditions are (1) a sufficiently high vacancy loop density, compared to the other sinks,[19,21–25] and (2) a sufficiently low yield of vacancy clusters in collision cascades.[21–25]

In these calculations, nevertheless, the number densities of interstitial clusters and loops are assumed to be constant.[23–25] As a result, the continuous generation of interstitial clusters in cascades only leads to the increase of the average size of existing loops.[23–25] This assumption is not easily justifiable, particularly at elevated temperatures, when a significant portion of defects is continuously produced in the form of immobile clusters. Indeed, the concentration of free vacancies in this case, due to the thermal instability of vacancy clusters, is significantly higher than that of free interstitials, causing the interstitial clusters and loops to shrink on average.[27] The evolution of the interstitial cluster population should therefore be described in a way similar to the shrinking vacancy clusters.[6,19–25] In other words, the Bullough-Eyre-Krishan (BEK) model,[28] originally developed for the vacancy clusters should also be applied to the interstitials clusters.[29]

Interstitial clusters directly produced in cascades are generally smaller in size than their vacancy counterpart. Due to their continuous generation and accumulation during cascade irradiation, they may have sink strengths higher than the vacancy clusters and loops. This is in contrast to the cases considered in Refs. 23–25, where the sink strength of interstitial clusters and loops is much smaller. Thus, the necessary condition for the instability derived there, i.e., a sufficiently high vacancy loop density compared to the other sinks, may never be applicable when both types of clusters are simultaneously produced.

In a previous paper,[26] we investigated the stability of a system of primary defects under cascade damage, with mobile point defects, vacancy loops, and sessile interstitial clusters. Through a linear stability analysis, we show that in a fully annealed metal a spatially homogeneous system of primary defects may still become unstable through the instability of the vacancy loop ensemble. The nontrivial conclusion that follows is that the instability occurs most easily, not at low, as it may be expected from Ref. 23, but rather at high clustering fraction ε_i of interstitials in cascades ($\varepsilon_i \cong 0.4$, Ref. 26). Indeed, although the higher fraction of interstitial

clustering in cascades increases the interstitial cluster number density, and restraints the instability development, yet it also produces higher net vacancy flux that helps build a higher sink strength of vacancy loops.[26]

In the present paper we carry our investigation further into the postbifurcation regime to consider the evolution of the heterogeneous microstructure from a homogeneous one under the continuous generation of mobile point defects, vacancy loops, and sessile interstitial clusters in collision cascades.

II. KINETIC MODEL

According to the BEK model,[28] the number of vacancies Q_{vl} accumulated in the shrinking vacancy loops can be described in terms of the following mean-field kinetic equation:

$$\frac{dQ_{vl}(t)}{dt} = \varepsilon_v G - \rho_{vl}[Z_{il}D_iC_i - Z_{vl}(D_vC_v - D_v\overline{C}_{vl})], \quad (1)$$

where G is the effective production rate of point defects in both clustered and free form, ε_v is the fraction of vacancies clustered in vacancy loops after the cascade collapse, D_j and C_j $(j=i,v)$ is the point-defect diffusion coefficients and mean-field concentrations, respectively, ρ_{vl} is the line density of vacancy loops, $\overline{C}_{vl}$ is the equilibrium concentration of vacancies in the neighborhood of vacancy loops, and Z_{jl} is the reaction constant between dislocation loops and point defects. The line density of vacancy loops is given by $\rho_{vl}=2Q_{vl}/(r_{vl}b)$ (b is the Burgers vector). The average vacancy loop radius r_{vl} is taken to be constant and equal to $r^0_{vl}/2$, where $r^0_{vl}=(n_{vg}\Omega/\pi b)^{1/2}$ is the initial radius of a vacancy loop, with n_{vg} and Ω being the number of vacancies in the loop at creation and the atomic volume, respectively.

We consider temperatures above annealing stage V at which the lifetime of vacancy clusters is governed mainly by vacancy emission from them. Consequently, there is a net vacancy flux to the sessile interstitial clusters, the total interstitial content Q_{ic} of which is described by a kinetic equation similar to (1),[26,29] i.e.,

$$\frac{dQ_{ic}(t)}{dt} = \varepsilon_i G - (1+\alpha)\rho_{ic}(Z_{vl}D_vC_v - Z_{il}D_iC_i), \quad (2)$$

where ε_i is the corresponding fraction of clustered interstitials, $\rho_{ic}=2Q_{ic}/r_{ic}b$ is the line density of interstitial clusters, which are treated as small loops of the average radius $r_{ic}=[r_{ic}(n_{ig})+r_{ic}(n_{i0})]/2$, $\alpha=n_{i0}/(n_{ig}-n_{i0})$. In deriving (2), the sessile primary interstitial clusters (PICs) are assumed to start with a uniform size of n_{ig} interstitials at the moment of creation.[29] They then shrink due to vacancy absorption, and below a minimum size n_{i0} of 4–5 interstitials they become mobile in a way similar to single interstitials.[30,31] Since the majority of interstitial clusters have, at the moment of creation, a size $n_{ig}\approx 6-10$ atoms,[32] $\alpha\approx 1$. On the other hand, vacancy loops are assumed to have bigger size at the point of creation ($n_{vg}\approx 30-50$), and the corresponding value of α in (1) is negligible.

In addition to the kinetic Eqs. (1) and (2), the conventional kinetic equations for the concentrations of the mobile species are also needed. In our present model, the mobile interstitial clusters are assumed to obey the same reaction kinetics as the single interstitials. The justification for this has been discussed previously.[33] Thus, interstitial clusters shrinking below the size n_{i0} are assumed to spontaneously dissolve, and the corresponding numbers of free point defects are added to the population of mobile single interstitials. Then, the conservation equations for the mobile vacancies and interstitials can be written as[26,29]

$$(1-\varepsilon_v)G - D_vC_v(Z_{vl}\rho_{ic} + Z_v\rho) - D_v(C_v - \overline{C}_{vl})Z_{vl}\rho_{vl} + D_v\nabla^2 C_v = 0, \quad (3)$$

$$(1-\varepsilon_i)G + \alpha D_vC_vZ_{vl}\rho_{ic} - D_iC_i(Z_{il}\rho_{vl} + Z_i\rho + (1+\alpha)Z_{il}\rho_{ic}) + D_i\nabla^2 C_i = 0. \quad (4)$$

Here ρ is the network dislocation density and Z_j is the reaction constant between point defects and network dislocations. To simplify further analysis we assume that $Z_{vl}=Z_v=1$, and $Z_{il}=Z_i\equiv Z=1+\eta$, to take into account the conventional dislocation bias. The additional influx j_{ic} of mobile interstitials in (4):

$$j_{ic} = \alpha\rho_{ic}(Z_{vl}D_vC_v - Z_{il}D_iC_i), \quad (5)$$

is due to the shrinkage of primary interstitial clusters PICs below the minimum size.[29]

It is easy to check that (1)–(4) satisfy the law of matter conservation, i.e.:

$$\frac{dQ_{ic}}{dt} = \frac{dQ_{vl}}{dt} + \rho(D_vC_v - ZD_iC_i) - \nabla^2(D_vC_v - D_iC_i). \quad (6)$$

Further, let us introduce the following "natural" notations related to the vacancy emission rate $D_v\overline{C}_{vl}$, which governs the lifetime of vacancy loops at elevated temperatures

$$\rho^0_{vl} = \frac{G[\varepsilon_v + \varepsilon_i/a(1+\alpha)]}{D_v\overline{C}_{vl}},\ Q_0 = \frac{G[\varepsilon_v + \varepsilon_i/a(1+\alpha)]r_vb}{2D_v\overline{C}_{vl}},$$

$$\rho^0_{ic} = a\rho^0_{vl}, \quad (7)$$

$$\tau = 2D_v\overline{C}_{vl}t/r_{vl}b = \frac{Gt[\varepsilon_v + \varepsilon_i/a(1+\alpha)]}{Q_0},\ \mathbf{x} = \mathbf{r}\sqrt{\rho^0_{vl}}, \quad (8)$$

$$Q_v = Q_{vl}/Q_0,\ Q_i = Q_{ic}/Q_0,\ \rho_N = \rho/\rho^0_{ic},$$

$$c_v = C_v/\overline{C}_{vl},\ c_i = D_iC_i/D_v\overline{C}_{vl}, \quad (9)$$

where $a=r_{vl}/r_{ic}$.

In these notations Eqs. (1)–(4) and (6) take the form

$$\frac{dQ_v}{d\tau} = \frac{\varepsilon_v}{[\varepsilon_v + \varepsilon_i/a(1+\alpha)]} - Q_v[Zc_i - (c_v - 1)], \quad (10)$$

$$\frac{dQ_i}{d\tau} = \frac{\varepsilon_i}{[\varepsilon_v + \varepsilon_i/a(1+\alpha)]} - a(1+\alpha)Q_i(c_v - Zc_i), \quad (11)$$

$$\frac{(1-\varepsilon_v)}{[\varepsilon_v+\varepsilon_i/a(1+\alpha)]}-ac_v(Q_i+\rho_N)-Q_v(c_v-1)+\nabla^2 c_v=0, \tag{12}$$

$$\frac{(1-\varepsilon_i)}{[\varepsilon_v+\varepsilon_i/a(1+\alpha)]}+\alpha a c_v Q_i-Zc_i[Q_v+(1+\alpha)aQ_i+a\rho_N]+\nabla^2 c_i=0, \tag{13}$$

$$\frac{dQ_i}{d\tau}=\frac{dQ_v}{d\tau}+a\rho_N(c_v-Zc_i)+\nabla^2(c_i-c_v). \tag{14}$$

From Eqs. (12) and (13), the net vacancy flux annihilated at interstitial clusters in a spatially homogeneous microstructure is equal to

$$c_v-Zc_i=\frac{(\varepsilon_i-\varepsilon_v)/[\varepsilon_v+\varepsilon_i/a(1+\alpha)]+Q_v}{Q_v+(1+\alpha)aQ_i+a\rho_N}, \tag{15}$$

so that the rate of accumulation of interstitials in clusters is given by

$$\frac{dQ_i}{d\tau}=\frac{\{\varepsilon_i(Q_v+a\rho_N)+\varepsilon_v(1+\alpha)aQ_i-[\varepsilon_v(1+\alpha)a+\varepsilon_i]Q_vQ_i\}}{[\varepsilon_v+\varepsilon_i/a(1+\alpha)][Q_v+(1+\alpha)aQ_i+a\rho_N]}. \tag{16}$$

In the absence of network dislocations ($\rho_N=0$), Eqs. (14) and (16) have a simple homogeneous solution $Q_v=Q_i=[1-\exp(-\tau)]$, which asymptotically approaches the stationary solution $Q_v=Q_i=1$. Since the net interstitial flux to the PICs (Zc_i-c_v) and the net vacancy flux to the PVCs (c_v-Zc_i-1) are both negative in this case [see Eq. (15) at $Q_v=Q_i=1$], both vacancy and interstitial clusters are shrinking on the average, which is consistent with our expectation from physical considerations.

If there is no interstitial clustering in collision cascades ($\varepsilon_i\equiv 0$), then, from Eqs. (14) and (15), the spatially homogeneous rate of vacancy accumulation in clusters is governed by the equation

$$\frac{dQ_v}{d\tau}=a\rho_N\frac{(1-Q_v)}{(Q_v+a\rho_N)}. \tag{17}$$

In Eq. (17) the stationary solution $Q_v=1$ corresponds to zero net interstitial flux to the dislocations, i.e., $Zc_i-c_v=0$.

When $Q_v=Q_i=1$ the total sink strength of small interstitial clusters $\rho_{ic}^0=2Q_0/r_{ic}b$ is larger than that of the vacancy loops $\rho_{vl}^0=2Q_0/r_{vl}b$ ($r_{vl}>r_{ic}$), as discussed in the introduction. Moreover, it follows from (11), (14), and (15) that when $\rho_N\neq 0$ more interstitials will be accumulated in the PICs than vacancies in the PVCs ($Q_i>Q_v$). In the latter case, due to the net vacancy flux at elevated temperatures ($c_v-Zc_i>0$), an extra number of free vacancies is absorbed by the network dislocations. Thus, the sink strength of PICs is generally higher than the sink strength of PVCs. This conclusion is contrary to that obtained in Ref. 23 where the interstitial loop number density was assumed to be stationary, so that, under the continuous PICs production in collision cascades, ρ_{vl} becomes much larger than ρ_{ic}.

III. INSTABILITY OF SPATIALLY HOMOGENEOUS SOLUTION

The evolution of small perturbations δQ_v and δQ_i of the steady-state spatially homogeneous solutions of Q_v and Q_i in (10) and (11), within the linear approximation, is governed by the equations

$$\frac{d\delta Q_v}{d\tau}=Q_v(\delta c_v-Z\delta c_i)+\left\{\frac{dQ_v}{d\tau}-\frac{\varepsilon_v}{[\varepsilon_v+\varepsilon_i/a(1+\alpha)]}\right\}\frac{\delta Q_v}{Q_v}, \tag{18}$$

$$\frac{d\delta Q_i}{d\tau}=-Q_i a(1+\alpha)(\delta c_v-Z\delta c_i)+\left\{\frac{dQ_i}{d\tau}-\frac{\varepsilon_i}{[\varepsilon_v+\varepsilon_i/a(1+\alpha)]}\right\}\frac{\delta Q_i}{Q_i}. \tag{19}$$

Neglecting high order terms of δQ_v and δQ_i, from (12) and (13), we have, for the Fourier components with the wave vector q:

$$\delta c_v-Z\delta c_i=\frac{(V\delta Q_v-I\delta Q_i)}{q^2+Z[Q_v+a\rho_N+a(1+\alpha)Q_i]}, \tag{20}$$

where

$$V=\frac{Z}{Q_v}\left\{\frac{\varepsilon_v}{[\varepsilon_v+\varepsilon_i/a(1+\alpha)]}-\frac{dQ_v}{d\tau}\right\}+\frac{(Z-1)(c_v-1)q^2}{Q_v+aQ_i+a\rho_N+q^2}, \tag{21}$$

$$I=\frac{Z}{Q_i}\left\{\frac{\varepsilon_i}{[\varepsilon_v+\varepsilon_i/a(1+\alpha)]}-\frac{dQ_i}{d\tau}\right\}-\frac{(Z-1)c_v q^2}{Q_v+aQ_i+a\rho_N+q^2}. \tag{22}$$

The homogeneous solution may become unstable when the determinant of the linear-evolution matrix of the system (18) and (19) changes its sign from positive to negative, meaning that one of the eigenvalues of the linear system becomes positive. The corresponding instability condition is given by

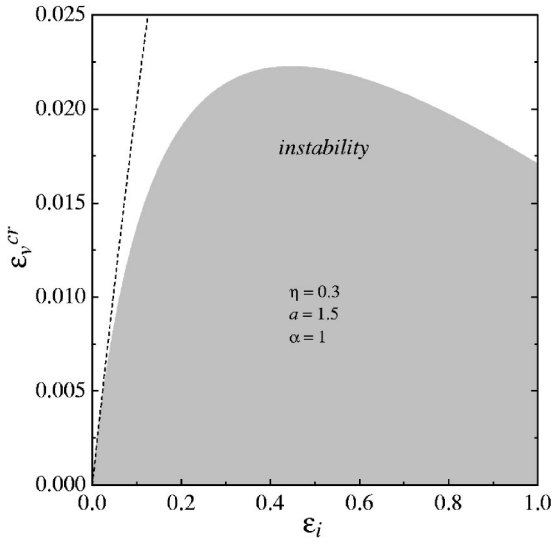

FIG. 1. Critical value of the vacancy clustering fraction as a function of interstitial clustering fraction. Dashed line corresponds to the limiting value of ε_v^{cr} at $\varepsilon_i \to 0 : \varepsilon_v^{cr} = \varepsilon_i / a^2(1+\alpha)$.

$$\frac{(Z-1)q^2}{Q_v + aQ_i + a\rho_N + q^2}\left[\frac{Q_v(c_v-1)}{Zc_i + 1 - c_v} - \frac{aQ_i c_v}{c_v - Zc_i}\right] \geqslant q^2 + Za\rho_N. \tag{23}$$

For the real values of q this condition can be fulfilled only if

$$(Z-1)\left[\frac{Q_v(c_v-1)}{Zc_i + 1 - c_v} - \frac{aQ_i c_v}{c_v - Zc_i}\right] \geqslant Q_v + aQ_i + a\rho_N(Z+1) + 2\sqrt{Za\rho_N(Q_v + aQ_i + a\rho_N)}. \tag{24}$$

At the critical point, i.e., when the largest eigenvalue vanishes, the wave vector q_{cr} for the unstable spatial modes is equal to

$$q_{cr}^2 = \sqrt{Za\rho_N(Q_v + aQ_i + a\rho_N)}. \tag{25}$$

For $\rho_N = 0$, the spatially homogeneous stationary solution is $Q_v = Q_i = 1$, and the inequality (23) reduces to that obtained before[26]

$$\frac{(Z-1)}{(q^2+1+a)(1+a)}\left\{\frac{1-(1+a)\varepsilon_v - \varepsilon_i/(1+\alpha)}{\varepsilon_v} - \frac{a[(1+\alpha)a + \varepsilon_i]}{\varepsilon_i}\right\} \geqslant 1. \tag{26}$$

The critical value of the vacancy clustering fraction ε_v^{cr}, below which the spatially homogeneous stationary solution $Q_v = Q_i = 1$ is unstable, can be easily calculated from (26). In Fig. 1, it is plotted as a function of interstitial clustering fraction ε_i. The critical wave vector q_{cr} is obviously equal to zero in this case, and for $\varepsilon_v < \varepsilon_v^{cr}$ the wave vectors of the growing spatial modes have an upper bound.[26] Note that ε_v^{cr} has its maximum around $\varepsilon_i \cong 0.4$.

The actual density of network dislocations is never zero, although its magnitude, as well as those of the densities of other sinks such as voids and gas bubbles, is usually small when the formation of spatially periodic arrays of defect clusters is observed.[12] In the presence of even low density of network dislocations, the spatially homogeneous solution of Eqs. (10)–(13) is not stationary. Since $dQ_i/d\tau > dQ_v/d\tau$ at $\rho_N \neq 0$, condition (24) can not be always satisfied as $\tau \to \infty$. However, as it follows from the conservation law (14), when $\rho_N \ll 1$, $Q_v(\tau) \cong Q_i(\tau)$ for $\tau \gg 1$. In this case, as we have seen in Sec. II, the spatially homogeneous vacancy and interstitial cluster contents exponentially approach the stationary value $Q_v = Q_i = 1$ with the characteristic time $\tau \sim 1$. As a result, from Eqs. (8) and (25), the critical wavelength of the unstable spatial modes can be approximately expressed through the line densities of network dislocations ρ and vacancy loops ρ_{vl}^0 as $(\rho\rho_{vl}^0)^{-1/4}$.

According to the foregoing paragraph, when $\rho_N \ll 1 (\rho \ll \rho_{vl}^0)$ the instability condition (24) will be fulfilled during the time period $\tau \gg 1$, if the inequality (26) is also satisfied. That this is really true is shown in Fig. 2, where the bifurcation parameter ζ, which is defined as the ratio of the right and left-hand sides of the inequality (24) minus one, is plotted as

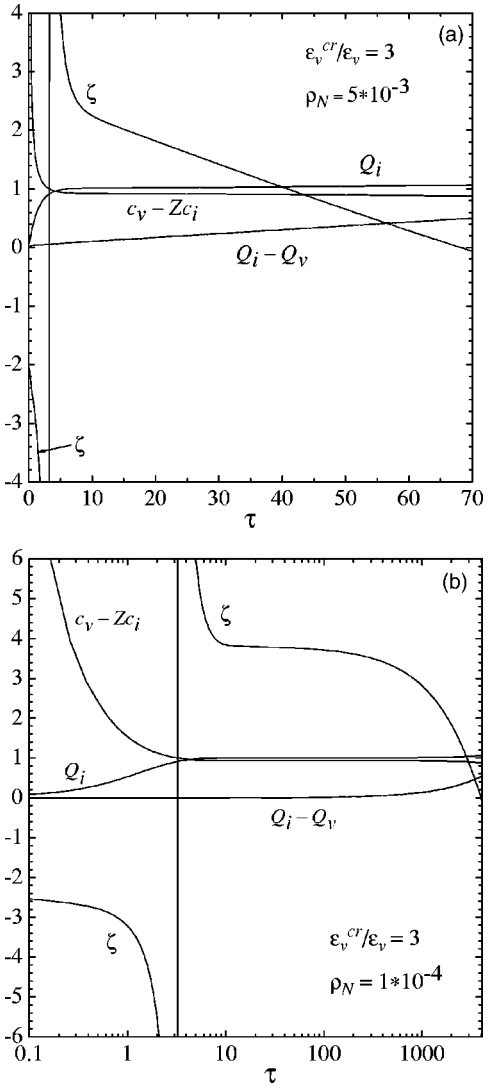

FIG. 2. Bifurcation parameter ζ and spatially homogeneous solution of Eqs. (10)–(13) as functions of time at different values of network dislocation density.

TABLE I. Material parameters for copper.

Parameter	Value
Atomic volume, Ω	1.0×10^{-29} m^3
Burgers vector, b	0.2 nm
Vacancy migration energy[a]	0.8 eV
Vacancy formation energy[a]	1.2 eV
Vacancy diffusivity pre-exponential[a]	1.0×10^{-5} m^2/s
Average loop line energy	0.2 eV
Initial vacancy loop radius	1 nm

[a]Reference 35.

a function of time. Here ζ is calculated for the spatially homogeneous solution $Q_j(\tau)$ of the set of Eqs. (10)–(13) with $\varepsilon_v<\varepsilon_v^{cr}$, where ε_v^{cr} is given by the equality in (26). Note that the value of $\rho_N=5\times10^{-3}$ in Fig. 2(a) does not necessarily represent a low network dislocation density. Indeed, the ordering of vacancy clusters is often observed under the ion irradiation.[12,13] Taking into account intracascade recombination, the characteristic nominal dose rate of ion irradiation $K\cong10^{-3}$ NRT dpa/s corresponds to an effective dose rate $G=1-2\times10^{-4}$ dpa/s.[34] Therefore, the value of $\rho_N=5\times10^{-3}$ in conventional units, for example in copper at 523 and 600 K, represents a network density of $\rho\approx2\times10^{15}$ and 2×10^{13} m^{-2}, respectively. This can be compared with the typical network density of 10^{13} m^{-2} in irradiated copper at elevated temperatures. The material parameters for copper are listed in Table I. In well-annealed pure copper the network density is below 10^{12} m^{-2}, i.e., ρ_N can be even lower than 10^{-5}. At $\rho_N=10^{-4}$, computer calculations give much longer period of time $\tau_{ins}=4\times10^3$, when the inequality (24) is fulfilled [Fig. 2(b)]. In copper this time period is equal to 8.9×10^6 and 5.3×10^4 s at 523 and 600 K, respectively.

The time τ_{ins} can be roughly estimated from the conservation law (14). The bifurcation parameter changes sign from positive to negative when the net vacancy flux to the network dislocations integrated over time becomes comparable with the amount of vacancies accumulated in vacancy clusters. Since $c_v-Zc_i\sim1$, $\tau_{ins}\approx(2a\rho_N)^{-1}$. The foregoing computer calculations support this estimation. Thus, in the presence of network dislocations, the instability of the spatially homogeneous solution may take place only within a finite time interval, and spatial heterogeneity, even if it develops, is not permanent. To check whether actually the development of spatial heterogeneity takes place under the instability condition (24), Eqs. (10)–(13) are solved numerically in the spatially inhomogeneous case.

IV. DEVELOPMENT OF SPATIAL HETEROGENIETY

A. Numerical results in one dimension

Weakly nonlinear analyses[21–23] and numerical calculations[24] show that in the postbifurcation regime the spatial pattern formation driven by the instability of the homogeneous vacancy loop population leads, after transients corresponding to three-dimensional patterns, to the eventual formation of planar wall defect structures. This conclusion is also supported by the experimental observations.[10–13] Therefore, we solve Eqs. (10)–(13) numerically for the one-dimensional case. The size of the computational cell L is taken to be 15–20 characteristic wavelengths defined by the Eq. (25) at $Q_v=Q_i=1$, and the fluxes of mobile defects are equal to zero at the cell boundaries. The accuracy of calculations is verified with the conservation law (14), written in the integral form

$$\int_0^L [Q_i(x,\tau)-Q_v(x,\tau)]dx = a\rho_N\int_0^\tau d\tau'\int_0^L [c_v(x,\tau')-Zc_i(x,\tau')]dx. \quad (27)$$

Typical spatial fragment of the solution is shown in Fig. 3 at the different moments of time. Similar to Ref. 24, the development of spatial heterogeneity leads to a sharpening of the concentration of vacancy clusters into walls, with very few clusters left in between. However, unlike Ref. 24, this is only true for the vacancy clusters. The spatial distribution of small interstitial clusters is much more homogeneous, and there is only some reduction of their concentration in the areas of sharp peaks of the vacancy cluster density. This is because even very inhomogeneous distribution of vacancy clusters has only a moderate effect on the spatial distributions of mobile defects. Since the homogeneous evolution of the interstitial clusters is stable itself, their spatial distribution just follows the spatial variations of the net interstitial flux $[Zc_i(x)-c_v(x)]$.

Concentrations of both mobile vacancies and interstitials decrease towards the peaks of the vacancy cluster concentration, as it should be, due to the higher total sink strength in the peak area (Fig. 4). However, the net vacancy flux (c_v-Zc_i) actually increases and, as a consequence, promotes the accumulation of vacancy clusters in the corresponding locations, and, at the same time, reduces the accumulation of interstitial clusters there. Moreover, the net vacancy flux (c_v-Zc_i) in the peak area approaches the value of unity, meaning the continuous accumulation of vacancy clusters with no practical shrinkage. Note that this result is not related to the interstitial clustering in collision cascades, although the clustering itself gives the net flux of vacancies $(c_v-Zc_i)\sim1$ already in the spatially homogeneous case [see Fig. 2 and Eq. (15)]. Similar calculations in the absence of interstitial clustering ($\varepsilon_i=0$), i.e., when the homogeneous net vacancy flux (c_v-Zc_i) is equal to zero [Eq. (15) at $\varepsilon_i=0$, $Q_v=1$], also show that $[c_v(x)-Zc_i(x)]\cong1$ at the peaks of vacancy cluster concentration.

Such behavior of the net vacancy flux in the peak areas is a result of the physical nature of the instability. Indeed, an increase in the vacancy cluster density diminishes the interstitial flux to the vacancy loops, promoting further accumulation of vacancies in clusters. On the other hand, the flux of mobile vacancies also decreases, opposing such accumulation. Due to the interstitial bias, the response of the interstitial flux overcomes that of the vacancy flux. As a result, for a sufficiently high dislocation bias, this positive feedback

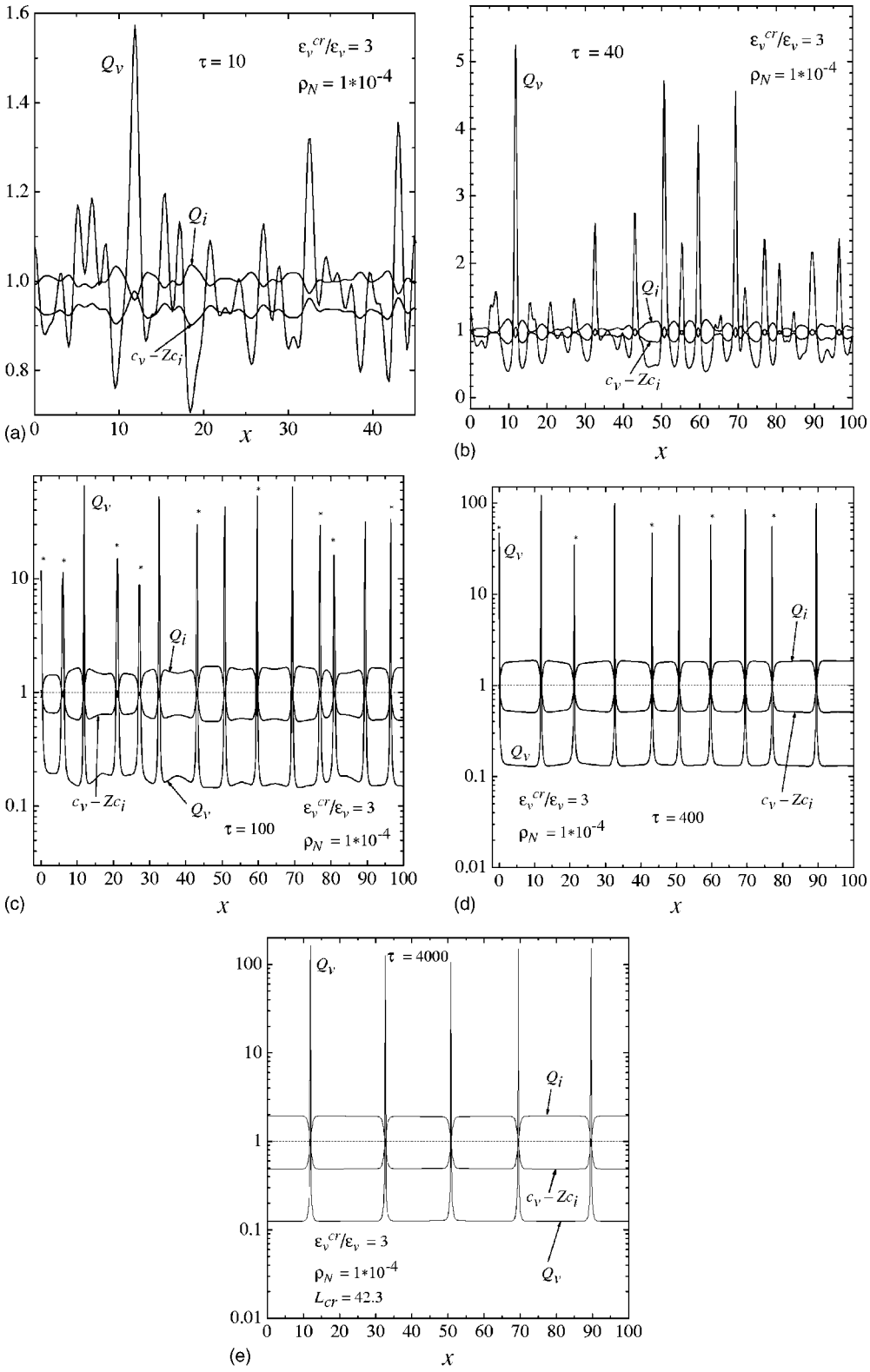

FIG. 3. Snapshots of spatial fragment of the inhomogeneous solution of Eqs. (10)–(13) under the instability conditions. Note that all peaks marked with asterisks disappear in the subsequent figures. L_{cr} is calculated with Eq. (25) at $Q_v = Q_i = 1$.

becomes strong enough to cause the instability and the development of a spatially ordered microstructure. Mathematically, the response of the net vacancy flux to a spatially inhomogeneous deviation of the vacancy cluster distribution is described by Eq. (21). Note that the second term of Eq. (21), which is proportional to the dislocation bias, is entirely responsible for the instability occurrence [see Eq. (24)].

The positive feedback between the accumulation of vacancy clusters in the peak areas and the corresponding increase in the net vacancy flux, discussed in the foregoing,

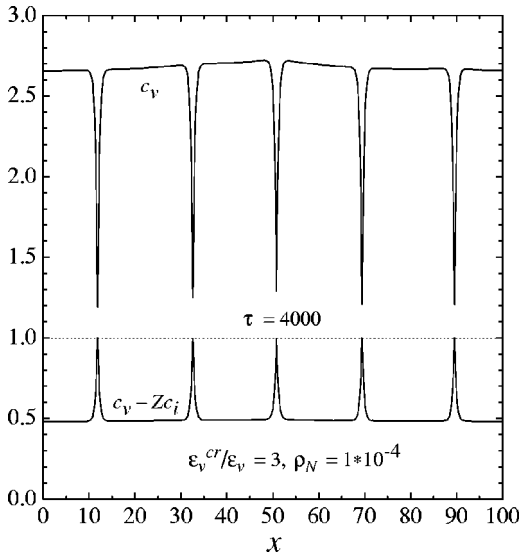

FIG. 4. Spatial behavior of the vacancy concentration c_v and the net vacancy flux $(c_v - Zc_i)$ for the case shown in Fig. 3(e).

may be operational only until the flux amplitude reaches a value of unity. Further operation would lead to the exponential growth of the cluster density in the peak areas with time [Eq. (10)]. Since the total number of clusters generated by irradiation in any finite volume can only increase linearly with time, the operation of the positive feedback mechanism is confined by the requirements of conservation law. How it actually happens is studied in more detail in the following subsection.

With time τ going beyond τ_{ins}, the homogeneous microstructure becomes stable again, and the spatial heterogeneity developed during earlier times has to eventually disappear. However, according to the numerical calculations [compare Figs. 2(a) and 5], the spatial heterogeneity may still survive for quite a long time after the instability condition (24) becomes invalid. In the example given in Fig. 5 the microstructure is homogeneous again at $\tau = 400$, which in copper at 523 and 600 K converts, in the conventional time scale, to $t = 8.9 \times 10^5$ and 5.3×10^3 (s), respectively. In the second case considered, i.e., when $\rho_N = 10^{-4}$, the damage microstructure homogenizes at $\tau \cong 2.3 \times 10^4$, which is also significantly larger than $\tau_{ins} = 4 \times 10^3$ [Fig. 2(b)]. In copper the time $\tau \cong 2.3 \times 10^4$ corresponds to $t = 5.1 \times 10^7$ and 3×10^5 (s) at 523 and 600 K, respectively.

B. Coarsening of concentration peaks

Simulating the peak distribution in Figs. 3 and 5, we consider the diffusion Eq. (12) within the one-dimensional spatial cell $[-l/2, l/2]$ of the length l:

$$\frac{(1-\varepsilon_v)}{[\varepsilon_v + \varepsilon_i/a(1+\alpha)]} + Q_v - k^2 c_v - Q_v'(c_v - 1)\delta(x) + \nabla^2 c_v = 0. \tag{28}$$

Here $\delta(x)$ is the δ function, which models the peak of the vacancy cluster density in the cell center. We also assume that the total sink strength $k^2 = a(Q_i + \rho_N) + Q_v$ outside of the peak area is approximately constant (see Figs. 3 and 5). With the zero-flux boundary conditions the solution of this equation can be written as (see the Appendix):

$$c_v - 1 = \frac{\{(1-\varepsilon_v)/[\varepsilon_v + \varepsilon_i/a(1+\alpha)] + Q_v - k^2\}}{k^2} \times \left\{ 1 - \frac{\cosh[k(x \pm l/2)]/\cosh(kl/2)}{1 + (2k/Q_v')\tanh(kl/2)} \right\}. \tag{29}$$

The plus and minus signs in expression (29) correspond to the negative and positive values of x, respectively.

According to Eqs. (10)–(16), (24), and (26), the value of parameter $\alpha = n_{i0}/(n_{ig} - n_{i0})$, which describes the additional influx of mobile interstitials due to the shrinkage of sessile interstitial clusters, only affects the instability threshold quantitatively. For a qualitative analyses of the spatial heterogeneity development, we can neglect this parameter, by setting, for example, $n_{i0} = 0$. As a result, inside the same spatial cell, the diffusion Eq. (13) for the concentration of mobile interstitials $c_i(x)$ will have a solution similar to (29), i.e.:

$$c_i(x) = \frac{(1-\varepsilon_i)/(\varepsilon_v + \varepsilon_i/a)}{Zk^2} \times \left\{ 1 - \frac{\cosh[\sqrt{Z}k(x \pm l/2)]/\cosh(\sqrt{Z}kl/2)}{1 + (2k/\sqrt{Z}Q_v')\tanh(\sqrt{Z}kl/2)} \right\}. \tag{30}$$

From Eqs. (29) and (30) the net vacancy flux received by vacancy clusters in the peak area is approximately

$$Q_v'[c_v(0) - 1 - Zc_i(0)] = \left\{ \frac{\varepsilon_i - \varepsilon_v}{\varepsilon_v + \varepsilon_i/a} - a(Q_i + \rho_N) + \frac{1-\varepsilon_i}{\varepsilon_v + \varepsilon_i/a}\left[1 - \frac{\tanh(\sqrt{Z}kl/2)}{\sqrt{Z}\tanh(kl/2)} \right] \right\} \times \frac{2\tanh(kl/2)}{k}. \tag{31}$$

In the derivation of (31), it is taken into account that $Q_v' \gg k$. Since $(\sqrt{Z} - 1) \ll 1$, we can further expand the right-hand side of Eq. (31) to get

$$Q_v'[c_v(0) - 1 - Zc_i(0)] = \left\{ \frac{\varepsilon_i - \varepsilon_v}{\varepsilon_v + \varepsilon_i/a} + \frac{(1-\varepsilon_i)(\sqrt{Z} - 1)}{\varepsilon_v + \varepsilon_i/a} \times \left[1 - \frac{kl}{\sinh(kl)} \right] - a(Q_i + \rho_N) \right\} \times \frac{2\tanh(kl/2)}{k}. \tag{32}$$

When $l > 3.5$ the ratio $kl/\sinh(kl) \ll 1$, and Eq. (32) reduces to

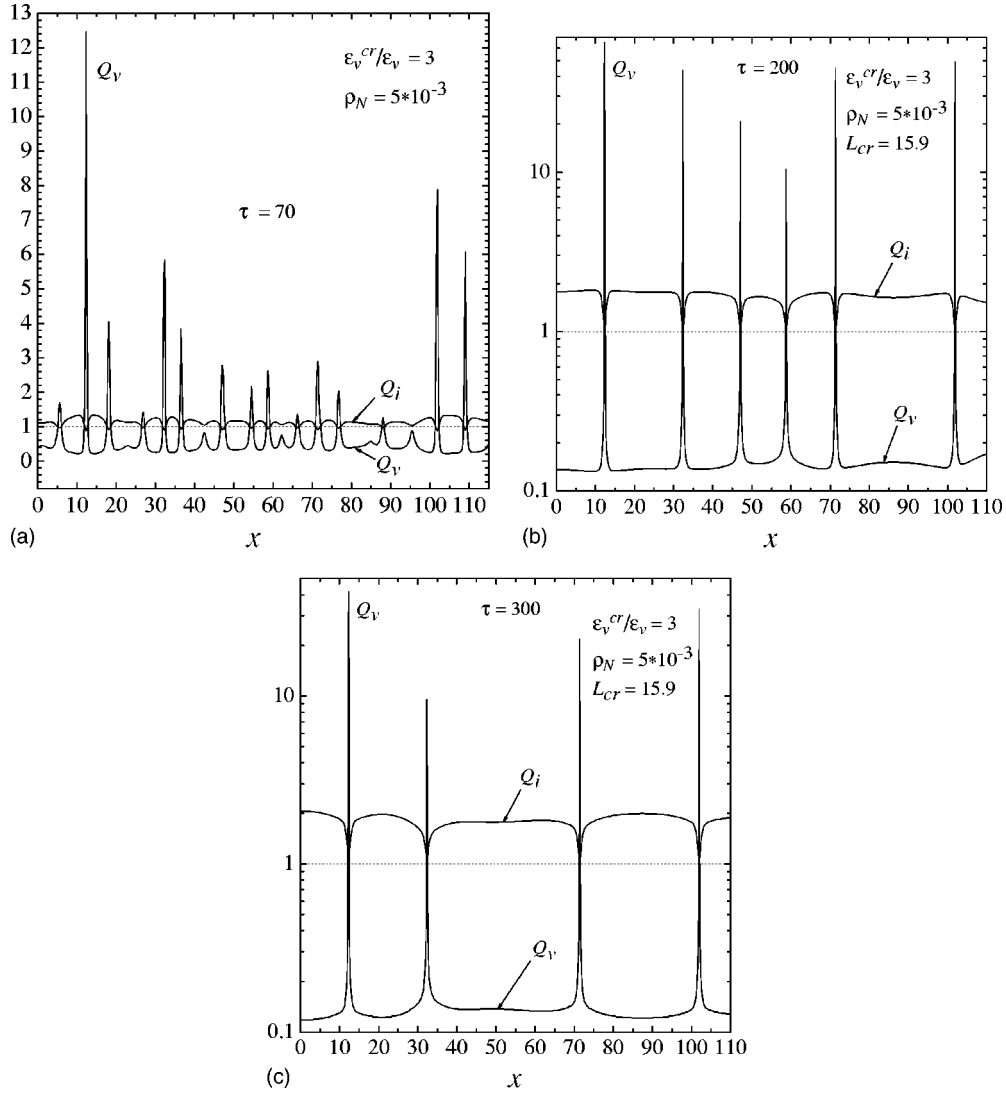

FIG. 5. Same as Fig. 3, but with higher network dislocation density.

$$Q_v'[c_v(0) - 1 - Zc_i(0)] = \frac{2}{k}\left[\frac{\varepsilon_i - \varepsilon_v + (1-\varepsilon_i)(\sqrt{Z}-1)}{\varepsilon_v + \varepsilon_i/a} - a(Q_i + \rho_N)\right]. \tag{33}$$

When the instability condition is satisfied, i.e., for $\tau < \tau_{ins}$, the conservation law (27) leads to $Q_i \approx Q_v'/l + Q_v$. According to Figs. 3(c), 3(d), and 3(e), we have $Q_i \gg Q_v$, meaning that practically all vacancy clusters are concentrated in the peak area. Thus, from Eqs. (10) and (33) it follows that the accumulation of vacancy clusters in the peak areas must saturate, unless the characteristic distance between the peaks l increases with time. This is exactly what we see in Fig. 3, where the height of some peaks continues to grow, while the neighboring peaks completely disappear. As a result of such coarsening effect, the remaining peaks of vacancy cluster concentration form an increasingly more regular spatial structure.

Equation (32) is also applicable when there is no interstitial clustering in collision cascades. Thus, at $\varepsilon_i = 0$ we have

$$Q_v'[c_v(0) - 1 - Zc_i(0)] = \frac{\sqrt{Z}-1}{\varepsilon_v}\left\{1 - \frac{kl}{\sinh(kl)} - \frac{(\varepsilon_v/\varepsilon_v^{cr})(\sqrt{Z}+1)}{Z[\sqrt{(1+a\rho_N)} + \sqrt{a\rho_N/Z}]^2}\right\} \times \frac{2\tanh(kl/2)}{k}. \tag{34}$$

Here we took into account that in the absence of interstitial clustering ($\varepsilon_i = 0$ and $Q_i = 0$) the instability condition (24) reduces to

$$\zeta = \frac{(Z-1)Q_v}{\varepsilon_v Z(1+a\rho_N)[\sqrt{(Q_v + a\rho_N)} + \sqrt{a\rho_N/Z}]^2} - 1 \geqslant 0. \tag{35}$$

The expression for parameter ε_v^{cr} is defined by the equality $\zeta(Q_v = 1, \varepsilon_v^{cr}) = 0$, and is similar to that obtained in Ref. 21.

For the conventional values of dislocation bias the ratio $(\sqrt{Z}+1)/Z > 1$, and, according to Eq. (34), no coarsening of

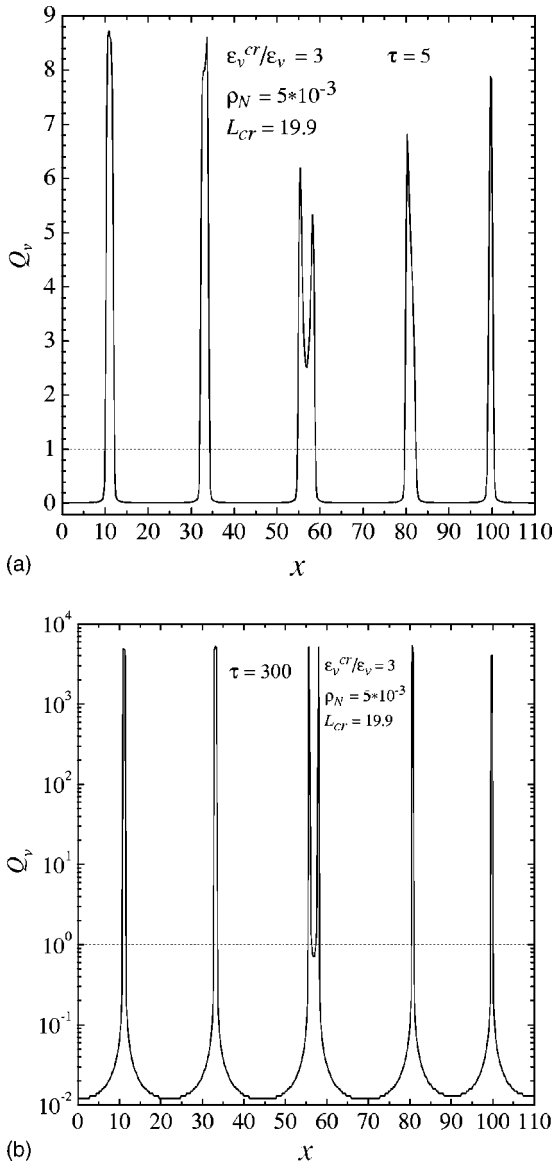

FIG. 6. Snapshots of spatial fragment of the inhomogeneous solution when there is no interstitial clustering ($\varepsilon_i = Q_i = 0$). L_{cr} is calculated with Eq. (25) at $Q_v = 1$, and $Q_i = 0$.

PVC distribution peaks should be expected when $\varepsilon_v/\varepsilon_v^{cr}$ is slightly below the unity. When $\varepsilon_v/\varepsilon_v^{cr}$ is significantly smaller than one, the peak coarsening does not happen either, because the reduction of the vacancy cluster concentration between the peaks only decreases the value of term $kl = (Q_v + a\rho_N)^{1/2} l$. On the contrary, if vacancy cluster concentration between the peaks is growing, i.e., k increases with time, the generation of additional concentration peaks, leading to the reduction of the distance l between peaks, may take place. The absence of peak coarsening at $\varepsilon_i = 0$ is illustrated in Fig. 6. That additional concentration peaks can appear in this case will be shown in the next section.

Although the interstitial clustering in cascades has been taken into account in Refs. 23 and 24, the evolution of the interstitial component of microstructure is treated very differently in the present paper, as mentioned in the introduction. Thus, in these papers, the interstitials in the immobile PICs directly produced in collision cascades are assumed to be equally distributed only among the existing interstitial loops (somehow avoiding the network dislocations and vacancy loops), the concentration of which was taken to be stationary.[23–25] As a result, the interstitial loops are not shrinking, but growing on the average, and their effect on the instability development is qualitatively the same as that of network dislocations.[23] Such a treatment is essentially equivalent to one in which there is no interstitial clustering. This explains why no peak coarsening was obtained in the previous numerical calculations.[20,24] Another consequence of the treatment of Refs. 23–25 is that the spatial heterogeneity developed at elevated temperatures is permanent, as long as the instability criteria (35) is fulfilled, while, according to the present approach, the spatial heterogeneity should be much less stable at these temperatures, and eventually disappears. The latter conclusion is supported by that the experimental observations of spatially periodic cluster arrays are restricted mostly to a rather narrow temperature range between annealing stages III and V.[12,13]

Concluding this section, we would like to return to its beginning and note the following. Similar to the particle scattering, where it is well known that a narrow three-dimensional potential barrier has a smaller effect on the particle motion, the response of concentrations of mobile defects to the sharp concentration peaks is weaker in the three-dimensional than in the one-dimensional case. Therefore, for the narrow peaks the positive feedback between the vacancy cluster density in the peak areas and the corresponding net vacancy flux is stronger in the one-dimensional case. It is interesting that in the three-dimensional case Eq. (28) does not even have the physical solution (see the Appendix). Thus, from the physics of the instability under consideration it follows that in the three dimensions the heterogeneous damage microstructure should indeed evolve towards the concentration of vacancy clusters in planar narrow walls.

Experimentally the walls of defect clusters are found to be arranged on {100} planes of the fcc lattice.[10–13] Together with the walls, voids are also observed sometimes. However, they are randomly distributed and do not participate in the ordering.[12,13] In this regard, it is worth noting that the one-dimensional migration of small self-interstitial clusters, which is observed in molecular dynamic simulations,[31] and often used to explain void-lattice formation,[36,37] takes place along the closed-packed directions, i.e., ⟨110⟩ in fcc metals. At the same time, it is shown in Ref. 24 that only 1% anisotropy in the diffusion coefficient of self-interstitials along a preferred direction (for example, ⟨100⟩) results in a significant alignment of clustered defects parallel to the directions of high mobility of the self-interstitials. Indeed, the correlation between the wall alignment and the directions of high mobility of the interstitials can also be predicted from the physics of the instability under consideration. The contradiction to the experimental observations indicates that the effective anisotropy of the interstitial diffusion must be small, so that the selection of the wall orientation is not controlled by the anisotropic transport of self-interstitial clusters, but rather, probably by the anisotropic elastic field of the defect clusters, through their effects on the interstitial fluxes. This apparent contradiction between the theoretical and experi-

mental (effective) transport properties of mobile interstitial clusters have been discussed and rationalized.[33] Since a small anisotropy can only slightly modify the instability conditions and does not affect the properties of the defect walls,[24,25] it is neglected in the present investigation.

V. LOW TEMPERATURE CASE

At temperatures when vacancy clusters are thermally stable, Eqs. (2) and (11) can no longer describe the evolution of primary interstitial clusters. At these temperatures, the PICs are not shrinking on the average, as it is assumed in Eq. (2), but are actually growing in size due to the net interstitial flux provided by the dislocation bias.[27] As a result of the growth of interstitial loops and their mutual coalescence with the subsequent dislocation network formation, the interstitial loop line density increases and approaches the saturation at a dose of 0.1 NRT dpa.[27] Microstructural investigations by transmission electron microscopy (TEM) during the early stages of the irradiation also indicate that already at doses $\sim$0.01 dpa self-interstitial atoms are absorbed by or create a dislocation network via loop formation and subsequent interaction of dislocation loops.[12,13] Similar to TEM, the experimental results obtained from the differential dilatometry demonstrate a continuous increase in specimen length with irradiation dose,[12,13] which reveals an efficient loss of self-interstitial atoms to an evolving dislocation network. Since the experimental observations also show that spatial fluctuations of the cluster density start to develop at $\approx$0.1 dpa,[12,13] for a qualitative description of the instability development we may use Eqs. (10)–(13), with ε_i and Q_i set to zero. In this case the parameter ρ_N represents the line density of both the network dislocations and the interstitial loops. Although, this simplification return us to the original simplest model,[20,21] we are not aware of any detailed study of what actually follows from this model at low temperatures.

Comparing the present approach with the model developed in Refs. 23–25, the following is noted. The assumption, that all the interstitials produced as immobile PICs are equally distributed among the existing interstitial loops,[23–25] literally means the introduction into the model the immobile PICs as the major driving force for the interstitial loop growth at low temperatures. This is contrary to the results of the more rigorous consideration,[27] where it was shown that in low temperature regime the interstitial loop growth is due to the dislocation bias. As far as the vacancy loop evolution is concerned, it is important to realize that the corresponding reduction of the flux of mobile interstitials leads to the overestimation of the lifetime of vacancy clusters and, as a result, their concentration. The latter is the crucial parameter for the instability development.

Formally, we can use the natural notations (7)–(9) for any temperature. However, since both ρ_{vl}^0 and the characteristic time τ are related to the rate of vacancy emission from vacancy clusters, they do not represent the corresponding physically meaningful values at low temperatures. This is because the vacancy emission rate is negligible in such cases. Indeed, in copper the formation of the dislocation walls have been experimentally observed at temperatures as low as 100 °C.[10–13] At this temperature, according to (7) and (8), $t=2\times10^{10}\tau$ (s), and $\rho_{vl}^0\cong2\times10^{21}$ m^{-2} ($G=10^{-7}$ dpa/s). Thus, the experimental doses of a few NRT dpa (Refs. 10–13) correspond to the values of τ well below 10^{-3}. Similarly, the physical values of vacancy cluster content Q_v is much less than unity. For such values of Q_v the spatially homogeneous Eq. (17) has the following simple solution:

$$\frac{Q_v(\tau)}{a\rho_N}=\sqrt{1+2\tau/a\rho_N}-1. \tag{36}$$

Substituting this expression into the instability condition (35), we obtain that the instability of spatially homogeneous solution sets in when

$$\frac{2\tau}{a\rho_N}+1=\left[\frac{1+\sqrt{1+(f_\varepsilon-1)(Zf_\varepsilon+1)}}{\sqrt{Z}(f_\varepsilon-1)}\right]^4, \tag{37}$$

and, from Eq. (25), the critical wavelength L_{cr} of unstable spatial modes is given by

$$L_{cr}=\frac{2\pi}{\sqrt[4]{Z\rho(\rho_{vl}+\rho)}}=\frac{2\pi}{\sqrt{\rho}}\left[\frac{(f_\varepsilon-1)}{1+\sqrt{1+(f_\varepsilon-1)(Zf_\varepsilon+1)}}\right]^{1/2}. \tag{38}$$

Here $f_\varepsilon=(Z-1)/(Z\varepsilon_v)$. Since $a\rho_N\ll1$, we have $f_\varepsilon=\varepsilon_v^{cr}/\varepsilon_v$. Note that the ratio $Q_v(\tau)/a\rho_N$ is equal to $\rho_{vl}(\tau)/\rho$ and does not depend on the rate of vacancy emission from vacancy clusters. The latter is also true for $\tau/a\rho_N=2\varepsilon_vGt/r_{vl}b\rho$. Since the term in square brackets of Eq. (38) weakly depends on the value of parameter f_ε, it varies from 0.56 to 0.86 when f_ε takes values from 2 to 10, the critical wavelength is mainly determined by the total line density of the interstitial loops and network dislocations ($L_{cr}\sim\rho^{-1/2}$). The experimental observations also show that the periodicity lengths of defect walls seem to be rather insensitive to temperature and defect production rate, in the sense that no clear dependence can be deduced from the existing data.[12]

Obviously, it is convenient for further analysis to rewrite Eqs. (10)–(13) in the following notations:

$$\overline{Q_v}=Q_v/a\rho_N,\ \overline{Q_i}=Q_i/\rho_N,\ \overline{c_j}=a\rho_Nc_j,\ \mathbf{x}=\mathbf{r}\sqrt{\rho},\ \overline{\tau}=\tau/a\rho_N. \tag{39}$$

As a result, the equations take the form

$$\frac{d\overline{Q_v}}{d\overline{\tau}}=\frac{\varepsilon_v}{[\varepsilon_v+\varepsilon_i/a(1+\alpha)]}-\overline{Q_v}[Z\overline{c_i}-(\overline{c_v}-a\rho_N)], \tag{40}$$

$$\frac{d\overline{Q_i}}{ad\overline{\tau}}=\frac{\varepsilon_i}{[\varepsilon_v+\varepsilon_i/a(1+\alpha)]}-(1+\alpha)\overline{Q_i}(\overline{c_v}-Z\overline{c_i}), \tag{41}$$

$$\frac{(1-\varepsilon_v)}{[\varepsilon_v+\varepsilon_i/a(1+\alpha)]}-\overline{c_v}(\overline{Q_i}+1)-\overline{Q_v}(\overline{c_v}-a\rho_N)+\nabla^2\overline{c_v}=0, \tag{42}$$

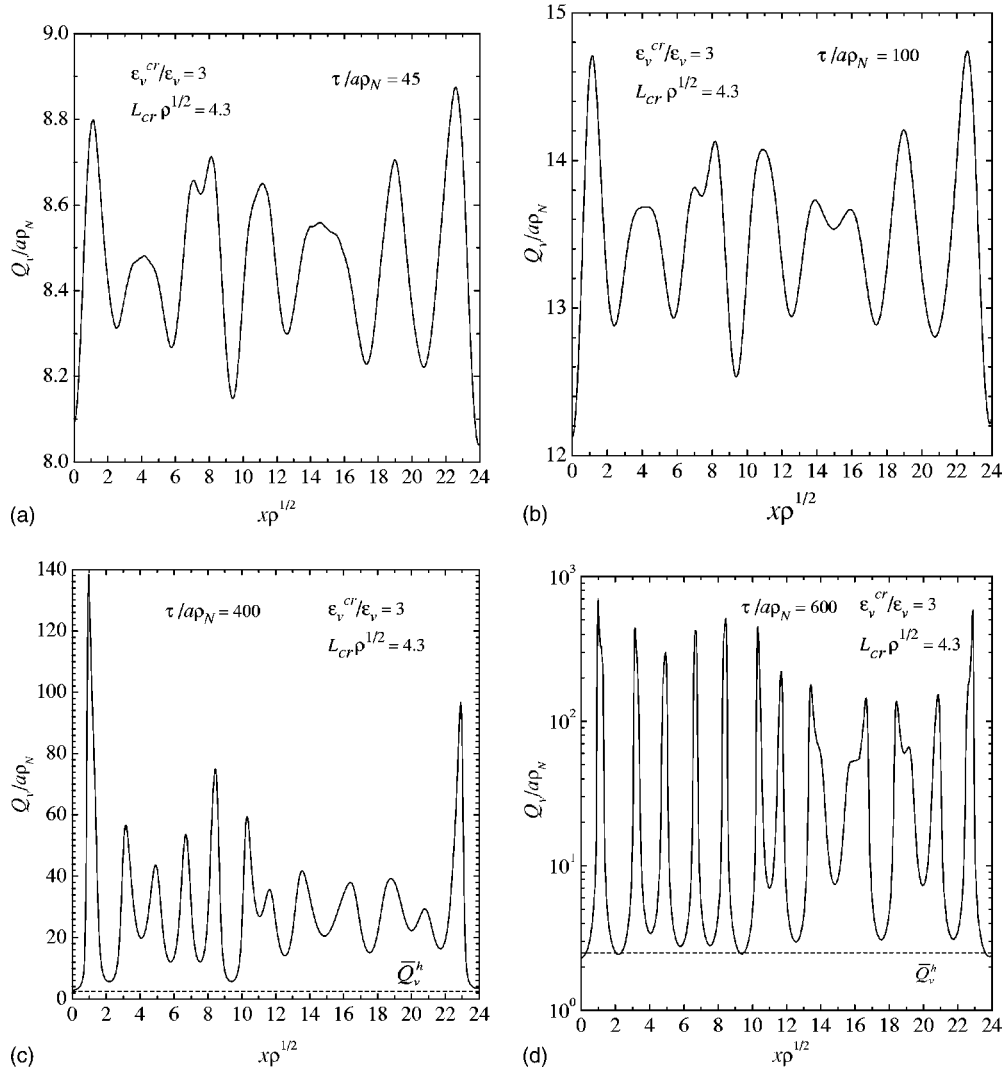

FIG. 7. Snapshots of spatial fragment of the inhomogeneous solution at low temperatures and $\varepsilon_i = Q_i = 0$. L_{cr} is calculated with Eq. (38).

$$\frac{(1-\varepsilon_i)}{[\varepsilon_v + \varepsilon_i/a(1+\alpha)]} + \alpha\overline{c_v}\,\overline{Q_i} - Z\overline{c_i}[\overline{Q_v} + (1+\alpha)\overline{Q_i} + 1] + \nabla^2\overline{c_i} = 0. \tag{43}$$

As we have seen in the foregoing, the vacancy emission term $a\rho_N$ in Eqs. (40) and (42) can be neglected, when vacancy clusters are thermally stable. Therefore, at the corresponding temperatures, unlike the elevated temperatures, the evolution of spatially heterogeneous microstructure governed by Eqs. (40)–(43) is universal, i.e., in agreement with experimental observations,[12] is independent of both the actual temperature and the dose rate. A typical example of the evolution is presented in Fig. 7.

From Eqs. (36) and (37), when $f_\varepsilon = 3$, the spatially homogeneous evolution becomes unstable at the time moment $\tau/a\rho_N = 5.7$, when $Q_v/a\rho_N = \overline{Q}_v^h = 2.5$. According to the figure, after the bifurcation, concentration of vacancy clusters initially grows everywhere in space, even between the peaks, where it is higher than the maximum value $\overline{Q}_v^h$ of the stable spatially homogeneous concentration of vacancy loops. In the previous paragraph we noted that in such circumstances additional peaks might appear. As it can be seen from the figure this scenario, which has not been observed in the previous numerical calculations,[20,24] is indeed realized. From the point of view of the stability analysis, such a behavior means that relatively smooth spatial variations of vacancy cluster concentration, corresponding to the wide peaks and wells, are also unstable, similar to the spatially homogeneous distribution. In Fourier space, this means that, due to the growth of the homogeneous value of Q_v, or, what is the same, the bifurcation parameter [see Eq. (35)], the wavelength of the fastest growing spatial mode, as defined by Eq. (25), becomes shorter. Note also that the spatial heterogeneity develops in such a way that, while the height of the peaks is growing, the vacancy cluster concentration between the peaks drops to values corresponding to a stable homogeneous solution, i.e., below $\overline{Q}_v^h$.

At low temperatures we do not actually take into account the interstitial clustering ($\varepsilon_i = 0$), and, consequently, a direct comparison between the present theoretical results and the

experimental data obtained under the ion irradiation, when a significant fraction of interstitials is generated in clusters, is not applicable. However, such comparison can be made in the case of 3 Mev protons,[10,13] when rather small cascades are most likely to be produced,[38] and, consequently, no direct formation of sessile interstitial clusters is expected. According to Fig. 7, the spatial periodicity in the vacancy cluster distribution with the spatial period l approximately equal to $2/\rho^{1/2}$ becomes very well developed already at the time $\tau/a\rho_N=600$. In copper at 100 °C the distance l between the defect walls is experimentally observed to be around 60 nm.[10,12,13] Since

$$\frac{\tau}{a\rho_N}=\frac{2\varepsilon_v Gt}{r_{vl}b\rho}=\frac{\varepsilon_v}{\varepsilon_v^{cr}}\frac{2Gt}{r_{vl}b(2/l)^2}\frac{Z-1}{Z}, \tag{44}$$

the time $\tau/a\rho_N=600$ corresponds to the dose $Gt\cong 0.4$ dpa ($Z=1.3$),[39] which, after taking into account that the defect survival probability in collision cascades is about 10%–20%,[32] is in a good agreement with the experimental value of 2–4 NRT dpa.[10–13]

One of the consequences of the production of rather small cascades under 3 MeV proton irradiation is also that the probability of cascade collapse into the vacancy cluster is relatively small as well. Therefore, the instability condition $\varepsilon_v<\varepsilon_v^{cr}$ can be fulfilled easier than under the neutron or ion irradiation. In this regard it is worth noting that under 3 MeV proton irradiation the most well-developed walls of defect clusters are experimentally found.[10,12,13] Under neutron and heavy ion irradiations mostly linear cluster arrays along cubic axes are reported. These cluster arrangements are similar to the precursors of wall formation observed at medium fluences under proton irradiation.[12]

VI. SUMMARY AND CONCLUSION

The evolution at elevated temperatures of a nonequilibrium system of primary defects produced continuously under cascade damage irradiation is studied. We analyzed a simple model in which the kinetics of small sessile interstitial clusters is treated in a way similar to the BEK model for shrinking vacancy loops. Development of spatial heterogeneity in this system is related to the instability of spatially homogeneous evolution of the vacancy loop population, caused by the positive feedback between the local vacancy cluster density and the interstitial flux.

A local increase in the vacancy cluster concentration diminishes the corresponding interstitial flux, promoting further accumulation of vacancies in clusters. For a sufficiently high dislocation bias, the response of the interstitial flux to the spatial variations of the vacancy cluster density is stronger than the corresponding damping effect of the vacancy flux. Under this condition, in the one-dimensional case considered the accumulation of vacancy clusters takes place in the narrow peaks separated by regions almost free of vacancy clusters. The feedback relation between the vacancy cluster concentrations and the interstitial flux towards them is stronger in the one-dimensional than in the three-dimensional case. Therefore, in the three-dimensional case the developing heterogeneous microstructure should correspond to the vacancy clusters concentrated in the narrow planar walls. This conclusion, which follows from the physics of the instability under consideration, agrees with the results of weakly nonlinear analysis[21–24] and the experimental data.[10–13]

As for the interstitial clusters, their spatial distribution remains much more homogeneous. There is only some reduction of their concentration in areas where the vacancy cluster density peaks, and the net vacancy flux is higher. In the case of interstitial clusters, there is no feedback relation between the cluster concentration and the fluxes of mobile defects, and the homogeneous evolution of the interstitial clusters is stable. Thus, their spatial distribution simply follows the spatial variations of the net interstitial flux.

At elevated temperatures, vacancy clusters are thermally unstable. In the presence of network dislocations, the sink strength of the interstitial cluster grows faster than that of vacancy clusters, with extra vacancies absorbed by the network. This allows the development of spatial heterogeneity when the network dislocation density is low, and only within a finite time period. During this period, the periodic spatial distribution of peaks of vacancy cluster density become increasingly better defined, due to ongoing peak coarsening, i.e., growth of peaks that satisfy the periodicity, and the complete dissolution of the neighboring ones. Although the evolving microstructure remains spatially heterogeneous long after the instability condition (24) becomes invalid, eventually homogeneity returns.

Peak coarsening does not occur, if the clusters produced in collision cascades are only vacancy in nature. Indeed, the number of concentration peaks may even increase with time, initially after the bifurcation. When the vacancy cluster density between concentration peaks drops to a value corresponding to the stable homogeneous solution, the spatial distribution of the peaks no longer changes. At lower temperatures, when vacancy clusters are thermally stable, the spatial distribution of the peaks is also independent of both the temperature and the damage rate. This is in agreement with the experimental observations.[12,13] At these temperatures interstitial clusters do not shrink on the average, but actually grow in size, because of the net interstitial flux provided by the dislocation bias. As a result of their growth and mutual coalescence, with the subsequent dislocation network formation, the interstitial loop line density almost saturates already at a dose of 0.1 NRT dpa.[27] Therefore, when vacancy clusters are thermally stable, qualitatively similar spatial behavior of the vacancy cluster density should be expected both with and without interstitial clustering in collision cascades.

If voids are present, the growth of interstitial loops from small sessile clusters directly produced in collision cascades is possible, with the formation of network dislocations at elevated temperatures subsequently.[27] Since the sink density of vacancy clusters at these temperatures is dictated by the rate of vacancy emission from them, it is usually much less than the total sink density of the interstitial clusters, loops, and the network dislocations.[27] In the presence of voids, the instability conditions also require that the sink density of vacancy clusters is larger than that of voids.[19,24] Conse-

quently, the condition for the instability of spatially homogeneous evolution given by Eq. (35) is difficult to realize in this case. In this regard, we note that the nonperiodic spatial segregation of voids and dislocation loops, with the interstitial loops concentrating in localized long narrow patches separated by void growth regions of size of about several microns,[14,15] is difficult to explain within the framework of the instability in the homogeneous vacancy loop population. Indeed, the total sink strength of the vacancy loops and stacking-fault tetrahedra, which are also present in such heterogeneous microstructure, is found to be much smaller than those of the voids and the interstitial loops.[15] Moreover, the spatial distribution of the vacancy clusters themselves is practically homogeneous.[15] As shown in Ref. 29, the instability of the homogeneous evolution in that case is related to the saturation of the homogeneous void growth, caused by the continuous production of small immobile interstitial clusters. The latter, being the major sinks almost from the start of irradiation, act as recombination centers for mobile defects and, as a result, suppress homogeneous development of the microstructure. The formation of the spatially heterogeneous microstructure in that case is caused by the spatial coarsening of the populations of voids, and the interstitial clusters and loops, instead.[29]

ACKNOWLEDGMENTS

The authors are grateful for funding support from the Hong Kong Research Grant Council (Research Grant Nos. PolyU 5173/01E, 5167/01E).

APPENDIX

For the negative values of x Eq. (28) with the zero-flux boundary conditions has the following solution:

$$c_v(x) = \frac{(1-\varepsilon_v)/[\varepsilon_v + \varepsilon_i/a(1+\alpha)] + Q_v}{k^2} - A\cosh[k(x+l/2)], \tag{A1}$$

where A is some constant, which has to be determined. For the positive values of x the solution is similar and given by

$$c_v(x) = \frac{(1-\varepsilon_v)/[\varepsilon_v + \varepsilon_i/a(1+\alpha)] + Q_v}{k^2} - A\cosh[k(x-l/2)]. \tag{A2}$$

Here it is taken into account that the vacancy concentration should be a continuous function at $x=0$. Further, integrating Eq. (28) over the infinitesimal interval around the initial point $x=0$, we get that the spatial derivative $c_v'(x)$ satisfies the equality

$$c_v'(+0) - c_v'(-0) = Q_v'[c_v(0) - 1]. \tag{A3}$$

Substituting Eqs. (A1) and (A2) into (A3), we arrive at

$$A = \frac{\{(1-\varepsilon_v)/[\varepsilon_v + \varepsilon_i/a(1+\alpha)] + Q_v - k^2\}}{k^2\cosh(kl/2)} \frac{1}{1 + (2k/Q_v')\tanh(kl/2)}. \tag{A4}$$

Equation (A4) together with Eqs. (A1) and (A2) gives the solution (29).

In the three-dimensional case Eq. (28) written for the concentration of mobile interstitials has the form

$$\frac{(1-\varepsilon_i)}{(\varepsilon_v + \varepsilon_i/a)} - Zk^2 c_i - ZQ_v' c_i \delta(\mathbf{r}) + \nabla^2 c_i = 0. \tag{A5}$$

For the spherical cell of the finite radius the general solution of Eq. (A5) is given by

$$c_i(r) = \frac{(1-\varepsilon_i)/(\varepsilon_v + \varepsilon_i/a)}{Zk^2} + \frac{A}{r}\exp(-\sqrt{Z}kr) + \frac{B}{r}\exp(\sqrt{Z}kr). \tag{A6}$$

Integrating (A5) over the infinitesimal spherical volume containing the initial point, we obtain that

$$4\pi(A+B) = -ZQ_v' \left[\frac{(1-\varepsilon_i)/(\varepsilon_v + \varepsilon_i/a)}{Zk^2} + \frac{A}{r}e^{-\sqrt{Z}kr} + \frac{B}{r}e^{\sqrt{Z}kr} \right]\Bigg|_{r\to 0}. \tag{A7}$$

From the latter equation it follows that

$$A = -B = \frac{(1-\varepsilon_i)/(\varepsilon_v + \varepsilon_i/a)}{2Z^{3/2}k^3}. \tag{A8}$$

As a result

$$c_i(r) = \frac{(1-\varepsilon_i)/(\varepsilon_v + \varepsilon_i/a)}{Zk^2}\left[1 - \frac{\sinh(\sqrt{Z}kr)}{\sqrt{Z}kr}\right] \leqslant 0. \tag{A9}$$

The interstitial concentration given by the last equation happens to be negative everywhere except the initial point $\mathbf{r}=0$, where it is equal to zero.

[1] P. Glansdorff and I. Prigogine, *Thermodynamic Theory of Structure, Stability and Fluctuations* (Wiley, New York, 1971).
[2] G. Nicolis and I. Prigogine, *Self-Organization in Non-Equilibrium Systems* (Wiley, New York, 1977).
[3] G. Haken, *Synergetics, An Introduction*, 2nd ed. (Springer, Berlin, 1978).
[4] G. Haken, *Synergetics. Instabilitiy Hierarchies of Self-Organizing Systems and Devices* (Springer, Berlin, 1983).
[5] I. Prigogine, *From Being to Becoming: Time and Complexity in Physical Sciences* (Freeman, San Francisco, 1980).
[6] K. Krishan, Radiat. Eff. **66**, 121 (1982).
[7] A. M. Stoneham, in *The Physics of Irradiation Produced Voids, Proceedings of Consulting Symposium*, edited by R. S. Nelson, Harwell Report No. AERE-R-7934, (1975, p. 319).
[8] L. D. Hullet, Jr., T. O. Baldwin, J. C. Crump, and F. W. Young, Jr., J. Appl. Phys. **39**, 3945 (1968).
[9] B. C. Larson and F. W. Young, Jr., in *Radiation Induced Voids in Metals*, edited by J. W. Corbett and L. C. Iannello (USAEC, Oak Ridge, TN, 1972), p. 672, CONF-710601.
[10] W. Jäger, P. Ehrhart, W. Schilling, F. Dworschak, A. A. Gadalla, and N. Tsukuda, Mater. Sci. Forum **15–18**, 881 (1987).
[11] W. Jäger, P. Ehrhart, and W. Schilling, in *Nonlinear Phenomena in Materials Science*, edited by G. Martin and L. P. Kubin (Transtech Aedermannsdorf, Switzerland, 1988), p. 279.
[12] W. Jäger, P. Ehrhart, and W. Schilling, Solid State Phenom. **3–4**, 297 (1988).
[13] W. Jäger, P. Ehrhart, and W. Schilling, Radiat. Eff. Defects Solids **113**, 201 (1990).
[14] B. N. Singh, T. Leffers, and A. Horsewell, Philos. Mag. A **53**, 233 (1986).
[15] C. A. English, B. L. Eyre, and J. W. Muncie, Philos. Mag. A **56**, 453 (1987).
[16] A. Jostons and K. Farrell, Radiat. Eff. **15**, 217 (1972).
[17] G. L. Kulcinski and J. L. Brimhall, in *Effects of Radiation on Substructure and Mechanical Properties in Metals and Alloys, American Society for Testing and Materials*, ASTM-STP 529 (ASTM, Philadelphia, 1973), p. 258.
[18] J. O. Steigler and K. Farrell, Scr. Metall. **8**, 651 (1974).
[19] E. A. Koptelov and A. A. Semenov, Phys. Status Solidi A **93**, K33 (1986).
[20] S. M. Murphy, Europhys. Lett. **3**, 1267 (1987).
[21] D. Walgraef and N. M. Ghoniem, Phys. Rev. B **39**, 8867 (1989).
[22] D. Walgraef and N. M. Ghoniem, Modell. Simul. Mater. Sci. Eng. **1**, 569 (1993).
[23] D. Walgraef and N. M. Ghoniem, Phys. Rev. B **52**, 3951 (1995).
[24] D. Walgraef, J. Lauzeral, and N. M. Ghoniem, Phys. Rev. B **53**, 14 782 (1996).
[25] D. Walgraef and N. M. Ghoniem, Phys. Rev. B **67**, 064103 (2003).
[26] A. A. Semenov and C. H. Woo, J. Phys. D **34**, 3500 (2001).
[27] A. A. Semenov and C. H. Woo, Appl. Phys. A: Mater. Sci. Process. **A67**, 193 (1998).
[28] R. Bullough, B. L. Eyre, and K. Krishan, Proc. R. Soc. London, Ser. A **346**, 81 (1975).
[29] A. A. Semenov and C. H. Woo, Appl. Phys. A: Mater. Sci. Process. **A74**, 639 (2002).
[30] P. Ehrhart, K. H. Robrock, and H. R. Schober, in *Physics of Radiation Damage in Crystals*, edited by R. A. Johnson and A. N. Orlov (Elsevier, Amsterdam, 1986).
[31] Yu. N. Osetsky, D. J. Bacon, A. Serra, B. N. Singh, and S. I. Golubov, J. Nucl. Mater. **276**, 65 (2000).
[32] D. J. Bacon, F. Gao, and Yu. N. Osetsky, J. Nucl. Mater. **276**, 1 (2000).
[33] S. L. Dudarev, A. A. Semenov, and C. H. Woo, Phys. Rev. B **67**, 094103 (2003).
[34] NRT dpa: displacement per atom defined according to M. J. Norgett, M. T. Robinson, and I. M. Torrens, Nucl. Eng. Des. **33**, 50 (1976); ASTM standards E521-83 (1983).
[35] H. E. Schaefer, in *Proceedings of the Sixth International Conference on Positron Annihilation, 1982*, edited by P. G. Coleman, S. C. Sharma, and L. M. Diana (North-Holland, Amsterdam, 1982), p. 369.
[36] C. H. Woo and W. Frank, J. Nucl. Mater. **137**, 7 (1985).
[37] H. L. Heinisch and B. N. Singh, Philos. Mag. **83**, 3661 (2003).
[38] A. J. E. Foreman, C. A. English, and W. J. Phythian, Philos. Mag. A **66**, 655, 671 (1992).
[39] B. C. Skinner and C. H. Woo, Phys. Rev. B **30**, 3084 (1984).